Steel and Composite Structures, *Vol. 24, No. 1 (2017) 37-52*
DOI: https://doi.org/10.12989/scs.2017.24.1.037

Seismic collapse probability of eccentrically braced steel frames

Yongsheng Qi *, Weiqing Li [a] and Ningning Feng [b]

Changzhou Key Lab of Construction Engineering Structure and Material Properties,
Changzhou Institute of Technology, No. 666, Liaohe Road, Changzhou City, Jiangsu Province, China

(*Received November 02, 2015, Revised February 25, 2017, Accepted February 28, 2017*)

Abstract. To quantitatively assess the safety against seismic collapse of eccentrically braced steel frame (EBSF) system, 24 typical EBSFs with *K*-shape and *V*-shape braces with seismic precautionary intensities 8 and 9 were designed complying with China seismic design code and relative codes to constitute archetype space of this structure system. In the archetype space, the collapse probability of the structural system under maximum considered earthquakes (MCE) was researched. The results show that the structures possess necessary safety against seismic collapse when they respectively encounter the maximum considered earthquakes corresponding to their seismic precautionary levels, and their collapse probabilities increase with increasing seismic precautionary intensities. Moreover, the EBSFs with *V*-shape braces have smaller collapse probability, thus greater capacity against seismic collapse than those with *K*-shape braces.

Keywords: seismic collapse; collapse probability; EBSF; IDA; rare earthquake

1. Introduction

Though eccentrically braced steel frames are widely used in China, the safety against seismic collapse of EBSFs, designed according to China code for seismic design of buildings and relative codes, has been scarcely researched. The paper aims to research the collapse probabilities of EBSFs under strong earthquakes.

The principle discovered by Ibarra *et al*. (2002) makes possible the assessment of seismic collapse of structures based on Probability Theory: the relationship between ground motion intensity and the collapse probability of a structure conforms with cumulative distribution function (CDF) of lognormal distribution. Once the relationship has been built, the collapse probability of a structure under certain earthquake intensity can be calculated so that the safety against seismic collapse of the structure can be quantitatively determined.

According to the principle, the Emergency Management Agency (FEMA) presented a methodology (FEMAP695 2008) to assess the safety against seismic collapse of structure system. Its main steps are as follows: (1) Design enough representative structures to constitute the archetype space for the structure system; (2) conduct incremental dynamic analysis for each archetype to determine collapse intensities under the 44 recommended earthquake waves; (3) Plot the collapse fragility curves according to the calculation results, then take account of uncertainty to modify them (uncertainty usually increase collapse risk); (4) According to the modified fragility curves, the collapse probabilities of all archetypes under maximum considered earthquake (corresponding to the rare intensity in seismic design code) can be calculated, then the safety against seismic collapse of the structure system can be assessed.

The relative researches are as follows. Chen and Mahin (2010) designed a series of double story X-braced steel frames using the provisions of ASCE-7/05 and analyzed their safety against seismic collapse according to FEMAP695. Shi (2009), Tang (Tang *et al*. 2010), Lu and Ye (2010, 2011) developed nonlinear procedure for collapse analysis and researched the collapse margin ratio, collapse cause of reinforced concrete frames and relative parameters. Li (2013) designed three groups of (3-, 6-, and 9-story) steel frames with different strong column coefficients, analyzed the influence of strong column coefficient on seismic collapse safety. Zhu (2013) studied the influence of local buckling on seismic collapse safety of steel frames. Gu (2013) took advantage of damage constitutive model to research responses of steel frames under strong earthquake and drew a conclusion that collapse occurs when the damage index reaches to critical value. Hsiao (2013) assessed the response modification coefficient of special concentrically braced frames and evaluated the collapse potential of the structural system. Qi (2012, 2015a) developed an automated control program for collapse assessment and researched the collapse criteria for BSF system. Yu (2014) analyzed the fragility-based probabilistic seismic safety assessment of RC frame structures with infilled masonry walls. Zheng (2015) used damage constitutive model to study the seismic capacity of steel frame structures. Qi (2015b) researched the safety against seismic collapse of concentrically braced steel frames and their phenomena of seismic collapse of weak story. Xu (2015) studied the seismic vulnerability of steel framework

*Corresponding author, Ph.D., Professor,
E-mail: Qiyongsheng621@163.com
[a] Ph.D.
[b] Ph.D.

ISSN: 1229-9367 (Print), 1598-6233 (Online)

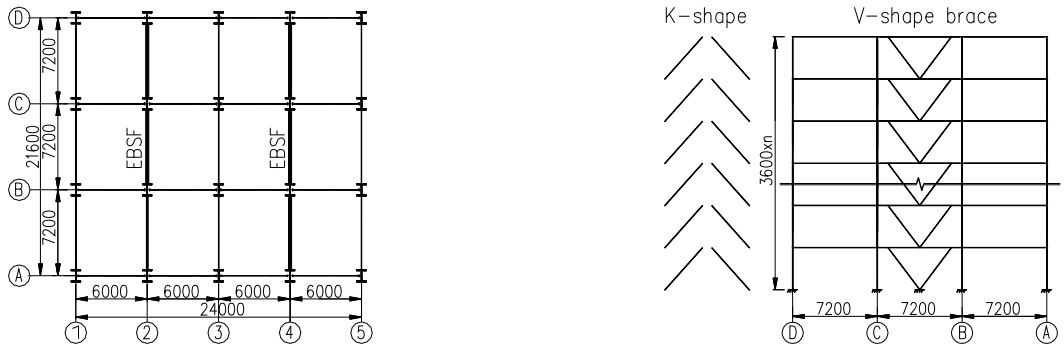

(a) Plan (b) Elevation

Fig. 1 Eccentrically braced steel frames

in service based on structural damage.

In the paper, 24 typical eccentrically braced steel frames with *K*-shape and *V*-shape braces are designed complying with China codes to constitute the archetype space, in which the collapse probability of the structure system is assessed according to FEMAP695 Methodology. Then the influences of story number of structures and seismic precautionary intensities on collapse probability are analyzed. At last, the seismic capacities of EBSFs with *K*-shape and *V*-shape braces are compared.

2. Archetype space

The design of EBSFs complies with the relative provisions in GB50011 (2010), GB50017 (2003), and GB50009 (2012), considers two cases of seismic precautionary intensities 8 and 9, including two kinds of brace types. The group with seismic precautionary intensity 8 contains 6-, 9-, 12-, 15-, and 18-story archetypes, and that of intensity 9 includes 6-, 9-, 12-, 15-, 18-, 24- and 30-story archetypes. The basic design accelerations of intensities 8, 9 are 0.2 and 0.4 g respectively. All the archetypes are located in the area of site class II, and belong to design earthquake group 1. Wind load is 0.4 kN/m^2, the live loads of roof and floor are 0.5 and 2.0 kN/m^2 respectively. The structural influencing coefficient R is 3.2.

The 6-story structure is made of Q235 steel, the rest is made of Q345 steel. The beams and braces take I-section, columns take I-section or box-section, and their gauges are summed up in appendixes 1 and 2.

The layout of the archetypes are shown in Fig. 1, all buildings are 3-span, 4-bay. The EBSFs are placed at axes 2 and 4, carrying total seismic action. The gravity load is averagely carried by 2 EBSFs and 3 moment-resisting steel frames (at axes 1, 3 and 5).

3. Numerical model and verification

3.1 Numerical model

Explicit finite element method is used to simulate the strongly nonlinear properties of structures during collapse process for its robust algorithm, ANSYS/LS-DYNA971 is chosen as the analysis tool. Hughes-Liu beam element is taken to simulate beams, columns, braces and welded beam-column joints, mass element to simulate lumped mass of the structure, Belytschko-Tsay shell element to simulate energy-dissipating beam-segment. The beam elements and shell elements are connected through rigid beam elements, as shown in Fig. 2.

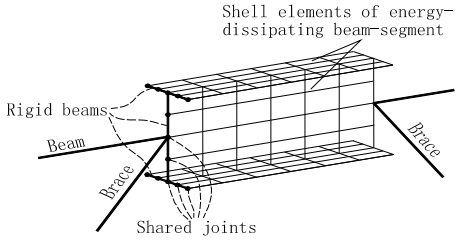

Fig. 2 Connection of beam elements and shell elements

Steel and weld metal both adopt Plastic Kinematic/ Isotropic material model, the third material model of LS-DYNA, which can take account of isotropic and kinematic hardening plasticity, especially material failure. This material model is very effective in large deformation analysis of steel structure.

The material properties of steel and weld metal are listed in Table 1 with the corresponding ANSYS/LS-DYNA commands. The data of Q235 and E43 weld metal adopt the test data of document (Gu 2009), those of Q345 and E50 weld metal are taken from GB/T1591 (2008) and GB/T5118 (1995).

Table 1 Material properties of steel and weld metal

Property	Q235	Q345	E43	E50
ρ (ton/mm^3)	7.85e-9	7.85e-9	7.85e-9	7.85e-9
E (MPa)	191268	200000	194953	194953
N	0.3	0.3	0.3	0.3
f_y (MPa)	235.3	345.6	330.6	390.8
E_t (MPa)	1073.8	959.1	1294	888.4
HP	0.2	0.2	0.2	0.2
FS	0.282	0.191	0.150	0.199

*Note: ρ is mass density, E is Young's modulus, v is Poisson's ratio, f_y is yield stress, E_t is tangent modulus, HP is hardening parameter, FS is failure strain

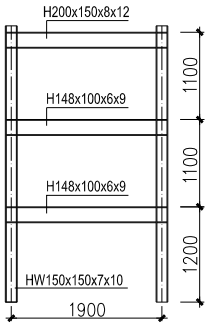

(a) Elevation

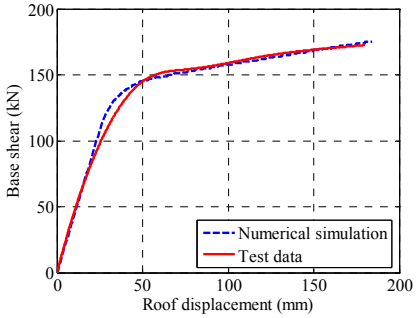

(b) Results of test and numerical simulation

Fig. 3 The first test

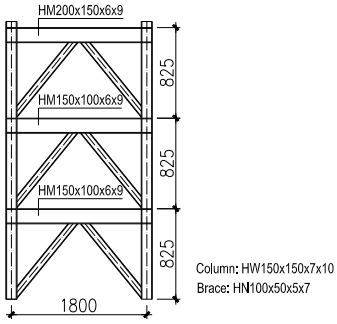

(a) Elevation

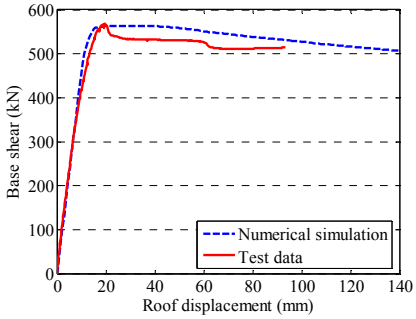

(b) Results of test and numerical simulation

Fig. 4 The second test

3.2 Numerical model verification

The applicability and exactness of the numerical model are testified by 10 simulation examples. For conciseness, only the simulation results about two destructive tests are provided here.

The first test is a Pushover test of three-story, one-span moment steel frame (shown in Fig. 3(a)). The simulation curve is consistent with the test curve at elastic stage (shown in Fig. 3(b)), then test curve enters yield stage prior to simulation curve because initial imperfects exist in the test model, the numerical model is ideal. But the two curves restore consistency at the hardening stage and keep it till the test ends.

The second test is a Pushover test of three-story, one-span K-braced steel frame (shown in Fig. 4(a)). Fig. 4(b) illustrates that the result of numerical stimulation agrees well with the test data at the elastic stage, and capture the point of ultimate bearing capacity with considerable precision, then simulate the decline stage of test curve with an acceptable deviation till the test ends.

The above analyses show that the numerical model possesses necessary nonlinear capacity and exactness to capture strength and stiffness degradation of structure under large deformation, satisfies the requirements of FEMAP695 for numerical model.

4. Collapse criterion

Qi (2014) quantitatively researched the ultimate capacity of deformation and collapse mechanism of braced steel frames (BSF) and argued that deformation and stiffness degradation double criteria can be used as the collapse criteria of BSF system. As for EBSF system, the concrete double criteria are: When one of the two phenomena happens, the structure is believed to reach to the critical state of collapse: (1) The slope of the IDA curve decreases to 5% of the initial slope. (2) The maximum interstory drift ratio exceeds 0.05 rad and 0.06 rad for *K*-shape and *V*-shape braced steel frames respectively.

5. IDA curves and fragility curves

Collapse analysis results include IDA curves and fragility curves. The IDA curves (for example, the Fig. 5(a) shows IDA results of EBSF EK-8-6) consist of 44 time-history response curves with increasing intensity of ground motion under 44 strong earthquake waves, and every little circle represent a time-history analysis. The '*' in every time-history response curve means that the deformation criterion controls the collapse analysis under the earthquake wave; the '☆' means that the stiffness degradation criterion governs the analysis. The x-coordinates of '*' and '☆' are the maximum interstory drift ratios of the structure, the *y*-coordinates are the values of PGA (Peak Ground Acceleration) of the earthquake waves when collapse occurs (in the paper, the intensity index of ground motion takes PGA).

The IDA results provide the collapse intensities of 44 earthquake waves, by which the fragility curve can be plotted (for example, the Fig. 5(b) shows the fragility curve

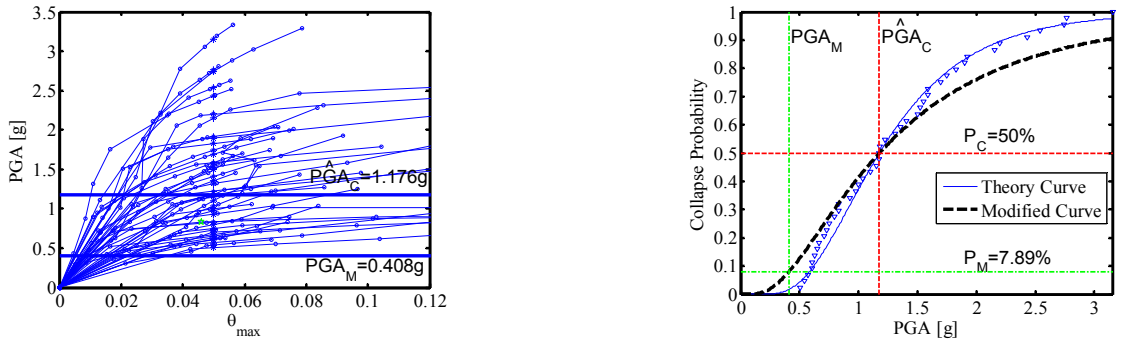

(a) IDA curves (b) Collapse fragility curve

Fig. 5 Collapse analysis results of EK-8-6

of EBSF EK-8-6). In the fragility curve, 44 '▽' are the collapse analysis results, and cumulative distribution function (CDF) curve of lognormal distribution is used to fit the data, which relate the collapse probability to earthquake intensity. The main two parameters of the function are the mean of the logarithms of the sample values, and the standard deviation of the natural logarithms of the sample values. The parameters can be defined as follows

$$\mu = \frac{\sum_{i=1}^{n}(Inx_i)}{n} \tag{1}$$

$$\beta = \sqrt{\frac{\sum_{i=1}^{n}(Inx_i - \mu)^2}{n-1}} \tag{2}$$

where, μ is the mean, β is the standard deviation, n is the sample number, and xi is the sample value, the collapse intensity corresponding to i^{th} earthquake wave.

The thin solid curve of fragility curves in Fig. 5(b) is the purely mathematic fitting curve, the thick dash line is the modified curve considering uncertain factors. FEMAP695 points out that the uncertainty generally increases the collapse risk, more uncertainty (corresponding to greater β value) means greater collapse probability. The uncertainty usually flattens the fragility curve.

The uncertainties in qualities of design requirements, model, test data contribute to variability in collapse safety. Larger variability in the overall collapse prediction will necessitate larger collapse margins in order to limit the collapse probability to an acceptable level at the MCE intensity.

(1) Quality of design requirements. GB50011 and GB50017 provide detailed design requirements, including computing method and seismic measures, which include research results for many years and lessons learned from a number of strong earthquakes, thus the quality of design requirements is categorized as 'B-Good'.

(2) Quality of test data. As shown in Section 3.2, structure tests can better validate the numerical model than member tests. The quality of test data in the study is categorized as 'B-Good'.

(3) Quality of numerical model. The explicit numerical model with bilinear constitutive relation considering material failure, can simulate yielding, buckling and fracture of members of EBSFs and the decline stage of bearing capacity curve. But the model of beam element cannot simulate the local buckling phenomena of plates and panel zone, so the quality of numerical model is categorized as 'C-Fair'.

FEMAP695 provide the following formula (3) to calculate the value of β_{TOT} to replace the purely mathematic β parameter.

$$\beta_{TOT} = \sqrt{\beta_{RTR}^2 + \beta_{DR}^2 + \beta_{TD}^2 + \beta_{MDL}^2} \tag{3}$$

where: β_{TOT} = total system collapse uncertainty;
β_{RTR} = record-to-record collapse uncertainty (0.40);
β_{DR} = design requirements-related collapse uncertainty (0.20-0.65);
β_{TD} = test data-related collapse uncertainty (0.20- 0.65);
β_{MDL} = modeling-related collapse uncertainty (0.20- 0.65).

For qualities B, B, and C of design requirements, test data and numerical model, β_{DR}, β_{TD} and β_{MDL} can be determined as 0.3, 0.3 and 0.45 respectively, thus β_{TOT} is equal to 0.74.

From fragility curve, the collapse probability of the structure corresponding to any intensity of ground motion can be determined, among which the most important data is the collapse probability of PGA_M. PGA_M is the value of PGA of maximum considered earthquake, corresponding to rare intensity (with a return period of 1600-2500 years) specified in seismic code, which is taken as 0.408g and 0.632 g respectively for seismic precautionary intensities 8 and 9.

The collapse analysis results of EK-8-6 (6-story eccentrically braced steel frame with *K*-shape braces in area with seismic precautionary intensity 8) are illustrated in Fig. 5.

The collapse analysis results of the rest 14 archetypes with seismic precautionary intensity 8 and all 12 archetypes of intensity 9 are illustrated in Appendixes 3 and 4 for compactness.

In addition, the horizontal lines of PGA_M and $\hat{PGA}_C$

Table 2 Collapse probability of EBSFs with seismic precautionary intensity 8

Archetype	P (%)	Archetype	P (%)
EK-8-6	7.89	EV-8-6	6.80
EK-8-9	5.67	EV-8-8	2.34
EK-8-12	5.35	EV-8-12	1.36
EK-8-15	2.68	EV-8-14	1.48
EK-8-18	3.05	EV-8-18	0.94
Average collapse probability (%) : 3.76			

* P: Collapse probability

Table 3 Collapse probability of EBSFs with seismic precautionary intensity 9

Archetype	P (%)	Archetype	P (%)
EK-9-6	16.80	EV-9-6	13.65
EK-9-9	13.52	EV-9-8	7.09
EK-9-12	8.28	EV-9-12	5.25
EK-9-15	8.86	EV-9-14	3.14
EK-9-18	10.11	EV-9-18	3.50
EK-9-24	4.61	EV-9-24	1.87
EK-9-30	4.52	EV-9-30	1.67
Average collapse probability (%) : 10.29			

$P\hat{G}A_C$ are depicted in IDA graph. $P\hat{G}A_C$ is the median of collapse intensities, used to define the CMR index of FEMAP695. The vertical lines of PGA_M and $P\hat{G}A_C$, and horizontal lines of corresponding collapse probabilities are plotted in the graph of fragility curve.

6. The seismic probability analysis of EBSF system

6.1 Seismic collapse probability

The probabilities of EBSFs of seismic precautionary intensities 8 and 9 are summarized in Tables 2 and 3 respectively. The data in Table 2 show that the probabilities of 10 archetypes with seismic precautionary intensity 8 are all less than 10%, and those of 40% of archetypes (EK-8-6, EK-8-9, EK-8-12, EV-8-6) are between 5.0% to 8.0%, and those of the rest 60% of archetypes are less than 5%. At the same time, the average of collapse probabilities of the design group with seismic precautionary intensity 8 is 3.76%.

FEMAP695 claims that the collapse probability of 20% for individual structure and that of 10% for structure system under strong earthquakes (maximum considered earthquake, corresponding to rare earthquake intensity) so that their capacity against seismic collapse meets the requirements of FEMAP695, furthermore, the EBSFs designed according to China Seismic Code in the areas with seismic precautionary intensity 8 possess considerable safety margin against seismic collapse.

Table 3 shows that the collapse probabilities of 14 archetypes with seismic precautionary intensity 9 are all less than 20%, and those of 28.6% of archetypes (EK-9-6, EK-9-9, EK-9-18, EV-9-6) are between 10.0% to 20.0%, and those of 28.6% of archetypes (EK-9-12, EK-9-15, EV-9-8 and EV-9-12) are between 5.0% to 10.0%, and those of 42.8% of archetypes (the rest) are less than 5%. At the same time, the average collapse probability of the design group with seismic precautionary intensity 9 is 10.29%, approximately equal to 10%, the acceptable collapse probability for structure system.

The data mean that the collapse probabilities of EBSFs designed according to China seismic design code in the areas with seismic precautionary intensity 9 basically meet the requirements of FEMAP695 and possess reliable safety against seismic collapse.

6.2 The relationship between collapse probability and story number

The relationship between collapse probability and story number are illustrated in Fig. 6. Collapse Probability-Story Number curves show two features.

(1) Collapse probabilities largely display declining tendency with the increase of intensity. The phenomenon means that the higher the structures are, their capacities against seismic collapse are stronger, which agrees with the general exception of engineers and society. In addition, in the

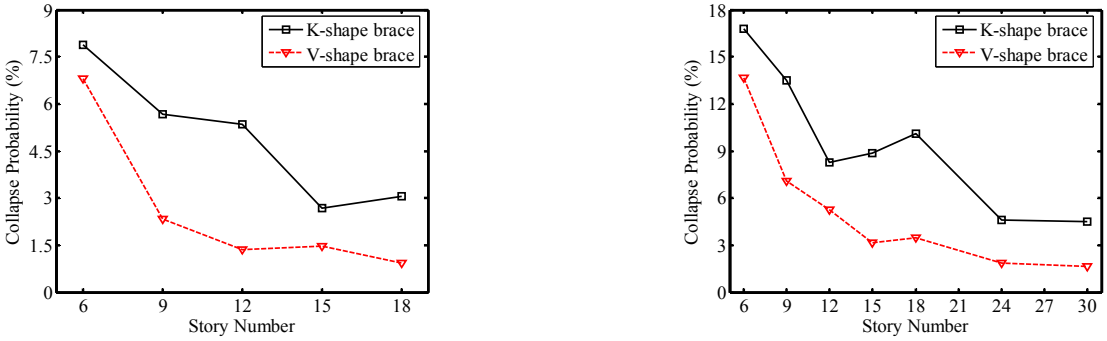

(a) Seismic precautionary intensity 8

(b) Seismic precautionary intensity 9

Fig. 6 The relationship of collapse probability with story number

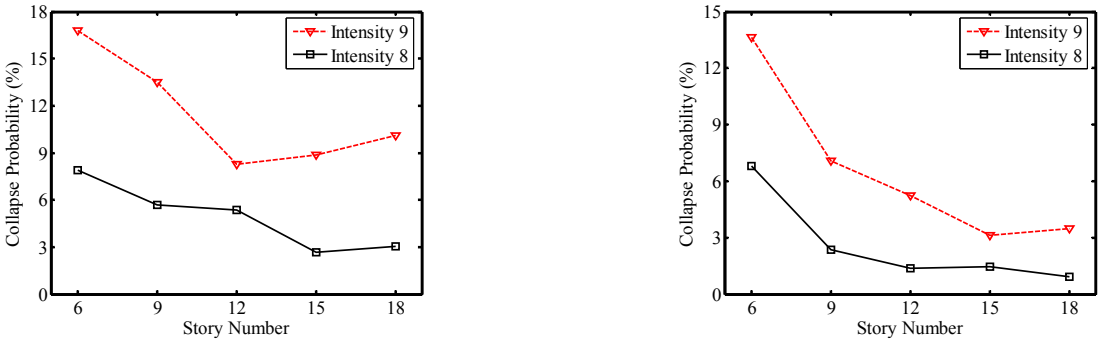

(a) EBSFs with *K*-shape braces (b) EBSFs with *V*-shape braces

Fig. 7 The relation of collapse probability with seismic precautionary intensity

designing of low-rise EBSFs, designers should take effective measures to appropriately improve their capacity against seismic collapse.

(2) In the total declining tendency of the 4 curves constituted by the collapse probabilities of 24 archetypes, there are 5 small fluctuations, occurring between EK-8-15 and EK-8-18, between EV-8-12 and EV-8-15, between EK-9-12 and EK-9-15, between EK-9-15 and EK-9-18, between EV-9-15 and EV-9-18. The exceptional fluctuations result from several reasons below.

Firstly, the reason of design leads to different margins of carrying capacity of different structures. Designers usually try to adjust member sections to assure safety and save steel, but the number of adjustments is limited and with a certain level of subjectivity, thus some lower structures may possess higher margins of capacity against seismic collapse.

Secondly, the natural period of a structure close to the predominant periods of most earthquake waves often results in early collapse because of similar resonance phenomenon. Conversely, the natural period far from the predominant periods of most earthquake waves postpone collapse. The factor may cause some exceptions of collapse phenomena.

Thirdly, the complexity of dynamic instability in IDA may cause the exceptional fluctuations of Collapse Probability-Number of Story curves. An important characteristic of dynamic instability lies that instability is the necessary condition, but not the sufficient condition, and only the instable vibration which cannot restore to stable state induces collapse. Whether or not the vibrating system can restore to stable state depends on original conditions, dynamic characteristics of the system when it is entering into the instable state, and on the properties and directions of loading. Some loading may make the system enduring an instable vibrating state restore to the stable state. Conversely, some loading may trigger collapse earlier.

In short, because of the three main reasons, the decreasing tendencies of collapse probability with story number is not consistent, some small fluctuations may exist in local stage of the curves.

6.3 The relationship between collapse probability and seismic precautionary intensity

The data and discussion of Section 6.1 suggests that the collapse probabilities of EBSFs are relative to the seismic precautionary intensity of the structures. The Figs. 7(a), (b) show that the collapse probabilities of archetypes with seismic precautionary intensity 8 are all less than those with intensity 9.

The main causes of the structures of higher seismic precautionary intensity possessing greater collapse probability are as follows.

The seismic code takes two methods to consider the increase of seismic action with the increase of seismic precautionary intensity: (1) The seismic influencing factor of structures, α_{max}. The maximum values of seismic influencing factor in seismic precautionary intensities 8 and 9 in seismic design code are 0.16 and 0.32; (2) Configuration measures. The structure members of higher seismic precautionary intensity require stricter configuration measures, including smaller slenderness ratio of braces and columns, smaller limit value of width-to-thickness ratio of plates. The effects of above method not only counteract the increasing seismic effects, but also endow the higher structures more safe margin.

The phenomenon reminds that stronger measures (for example, greater seismic influencing factor of structures, smaller structural influencing coefficient, and stricter configuration requirements) should be taken to decrease the collapse probability of structures in zones of high seismic precautionary intensity.

In addition, the realistic design provisions should assure structures possess proximately equal collapse probability for similar structures in zones of different seismic precautionary intensities. How to realize the objective in design is a valuable research direction.

6.4 The influences on seismic property of energy-dissipating beam-segment

In Section 6.2, Fig. 6 shows that the EBSFs with V-shape braces possess smaller collapse probability than EBSFs with *K*-shape braces. The average values of collapse probabilities of EBSFs with *V*-shape and *V*-shape braces are 4.92% and 2.58% for the seismic precautionary intensity 8, and those are 9.53% and 5.17% for the seismic precautionary intensity 9 respectively. The difference of seismic property is related with energy-dissipating beam-segments.

As the ‘fuse members’ of EBSF system, the energy-

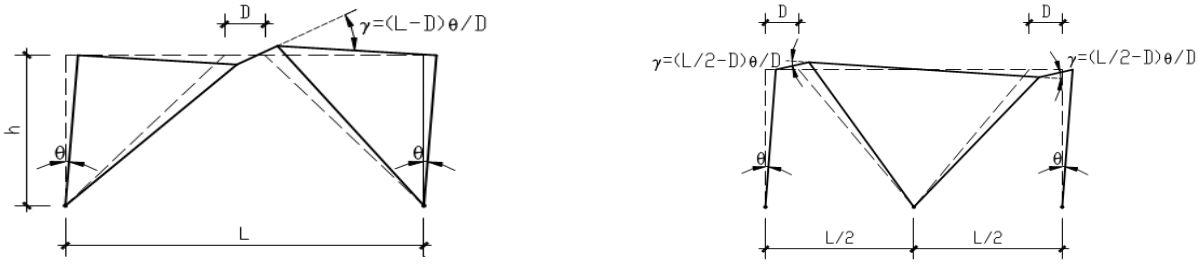

(a) *K*-shape brace (b) *V*-shape brace

Fig. 8 Horizontal deformations of EBSFs

dissipating beam-segments play the role of absorbing and dissipating earthquake energy, decreasing seismic effect to protect the main structure. The different energy-dissipating beam-segments resulting from different brace types remarkably affect the seismic property. The following analyses compare the seismic properties of two kinds of EBSFs in the paper.

The one-span, one-story eccentrically braced steel frames with different brace types are shown in Fig. 8. The EBSF in Fig. 8(a) with *K*-shape brace possess one energy-dissipating beam-segment, the EBSF in Fig. 8(b) with V-shape brace possess two energy-dissipating beam-segments. The span is L, the height is h, the lengths of energy-dissipating beam-segments are all D. Apply a same horizontal displacement at the roof of each EBSF, and assume that the deformations concentrate in energy-dissipating beam-segment, the columns all rotate a same angle θ, the energy-dissipating beam-segment of K-braced structure generates the shear angle $\gamma_K = (L - D)\,\theta/D$, and those of V-braced structure generate the shear angle $\gamma_V = (L/2 - D)\,\theta/D$. The shear angle of V-braced structure is obviously less than that of K-braced structure, and the difference is $\Delta\gamma = (L-D)\,\theta/D - (L/2-D)\,\theta/D = L\theta/(2D)$. Taking D as L/9, the ratio $\gamma_V / \gamma_K = [(L/2-D)\,\theta/D] / [(L-D)\,\theta/D] = 0.438$. Namely, the shear deformation of energy-dissipating beam-segments of V-braced structure is less than a half of that of K-braced structure. Thus it can be seen, if other conditions are same, the V-braced EBSF can endure more horizontal deformation than K-braced EBSF, dissipate more earthquake energy so that can be expected to possess more excellent seismic property and low collapse probability.

7. Conclusions

This study designed 24 representative eccentrically braced steel frames with *K*-shape and *V*-shape braces according to China code for seismic design of buildings and related codes, by which the collapse probability of the structure system is researched, the conclusion are as follows.

- The collapse probabilities of all archetypes under maximum considered earthquakes are less than the 20%. The average value of collapse probabilities of EBSFs of seismic precautionary intensities 8 is less 4% and that of intensity 9 is approximately equal to 10%. The results meet the requirements of FEMAP695 Methodology so that EBSFs designed complying with design frame of current China design codes are safe under rare earthquakes.
- The collapse probabilities of EBSFs decrease with increasing story number when subjected to strong earthquakes.
- The collapse probabilities of EBSFs of seismic precautionary intensity 8 are larger than those of intensity 9.
- The EBSFs with *V*-shape braces possess smaller collapse probability, thus more excellent structural properties than those with *K*-shape braces.

Acknowledgments

The study was financially supported by Science and Technology Plan Project of Changzhou City, 'Research on collapse probability and collapse mechanism of concentrically braced steel frames under strong earth-quakes' (CJ20159031), the Research Project of Ministry of Housing and Urban-Rural Development 2014-K2-038.

References

Chen, C.H. and Mahin, S. (2010), "Seismic collapse performance of concentrically steel braced frames", *Proceedings of 2010 ASCE Structures Congress*, Orlando, FL, USA, May.

FEMA (2008), FEMAP695, Federal Emergency Management Agency; Quantification of building seismic performance factors, Washington, D.C., USA.

GB/T1591-2008 (2008), High strength low alloy structural steels; Beijing, China.

GB/T5118-1995 (1995), Low alloy steel covered electrodes; Beijing, China.

GB50009-2012 (2012), Ministry of Housing and Urban-Rural Development; Load code for design of building structures, Beijing, China.

GB50011-2010 (2010), Ministry of Housing and Urban-Rural Development; Code for seismic design of buildings, Beijing, China.

GB50017-2003 (2003), Ministry of Construction; Code for design of steel structures, Beijing, China.

Gu, Q. (2009), *Hysteretic Properties and Seismic Design of Steel Structures*, China Architecture & Building Press, Beijing, China.

Gu, L. (2013), "Collapse displacement analysis of the steel frame structure based on the damage index", Master Degree Dissertation; Suzhou College of Science and Technology, Suzhou, China.

Hsiao, P.C. (2013), "Evaluation of the response modification

coefficient and collapse potential of special concentrically braced frames", *Earthq. Eng. Struct. Dyn.*, **42**(10), 1547-1564.
Ibarra, L.F., Media, R.A. and Krawinkler, H. (2002), "Collapse assessment of deteriorating SDOF systems", *Proceedings of the 12th European conference on Earthquake Engineering*, London, UK, September.
Li, D. (2013), "Anti-collapse analysis of steel frame with different strong column coefficient", Master Degree Dissertation; Suzhou College of Science and Technology, Suzhou, China.
Liel, A.B. (2008), "Assessing the collapse risk of California's existing reinforced concrete frame structures: Metrics for seismic safety decisions", Stanford University, Stanford, CA, USA.
Lu, X. and Tang, D. (2011), "Study on the seismic collapse resistance of RC frame structures with equal spans in zones with seismic intensity VII", *J. Earthq. Eng. Vib.*, **31**(5), 13-20.
Lu, X. and Ye, L. (2010), "Study on the seismic collapse resistance of structural system", *Earthq. Resist. Eng. Retrofit.*, **32**(1), 13-18.
Lu, X. and Ye, L. (2011), "Seismic damage simulation and analysis of typical RC frames of Xuankou school", *Eng. Mech.*, **28**(5), 71-77.
Qi, Y. (2012), "Efficient and automated method of collapse assessment", *Steel Compos. Struct., Int. J.*, **13**(6), 561-570.
Qi, Y. (2014), "Research on seismic collapse margin ratio of braced steel frame considering structural influencing coefficient", Ph.D. Dissertation; Hohai University, Nanjing, China.
Qi, Y. (2015a), "Automated collapse assessment method based on Matlab and software interface technology", *Architect. Technol.*, **46**(11), 1042-1045.
Qi, Y. (2015b), "Phenomenon of seismic collapse of weak story of CBSFs", *J. Hefei Univ. Technol.*, **38**(12), 75-84.
Shi, W. (2009), "Study on the collapse-resistant capacity of RC frames with different seismic fortification levels", *Proceedings of the 12th Conference on Seismic Technology of High-Rise Buildings & 60th Anniversary Symposium of Beijing Institute of Architectural Design & Research*, Beijing, China, October. [In Chinese]
Tang, D., Lu, X., Ye, L. and Shi, W. (2010), "Influence of axial compression ratio to the seismic collapse resistance of RC frame structures", *Earthq. Resist. Eng. Retrofit.*, **32**(5), 26-35.
Xu, Q. (2015), "Seismic vulnerability of steel framework in service based on structural damage", *J. Vib. Shock*, **34**(6), 162-167.
Yu, X.H. (2014), "Fragility-based probabilistic seismic safety assessment of RC frame structures with infilled masonry walls", *Civil Eng. J.*, **47**(2), 260-265.
Zheng, S.S. (2015), "Seismic capacity analysis for steel frame structures considering cumulative damage", *Civil Build. Struct.*, **45**(10), 32-37.
Zhu, L. (2013), "Study on the collapse resistance capacity of steel frames considering local buckling of columns", Master Degree Dissertation; Suzhou College of Science and Technology, Suzhou, China.

Appendix 1 Member sections of archetypes of seismic precautionary intensity 8

Name	Story	Exterior column	Interior column	Exterior beam	Interior beam	Brace
EK-8-6 EV-8-6	4-6	I300×210×10×12	I450×240×10×14	I400×220×10×14	I400×220×10×14	I170×170×10×10
	1-3	I350×240×10×14	I450×270×12×20	I400×220×10×14	I400×220×10×14	I170×170×10×12
EK-8-9 EV-8-9	7-9	I300×190×10×14	I350×200×10×14	I300×200×10×16	I300×200×10×16	I170×170×10×12
	4-6	I300×220×10×14	I450×250×14×16	I300×240×10×16	I300×240×10×16	I180×180×12×12
	1-3	I350×250×10×16	I450×300×14×20	I300×240×10×16	I300×240×10×16	I190×190×12×12
EK-8-12 EV-8-12	10-12	I300×200×10×14	I350×200×10×14	I300×200×10×16	I300×200×10×16	I170×170×8×12
	7-9	I350×220×10×14	I450×250×12×16	I300×200×10×16	I300×200×10×16	I170×170×10×12
	4-6	I350×280×10×16	I500×320×14×18	I300×240×10×18	I300×240×10×18	I180×180×12×12
	1-3	I350×300×12×18	I500×360×16×22	I300×240×10×18	I300×240×10×18	I190×190×12×12
EK-8-15 EV-8-15	13-15	I250×230×10×16	I250×230×10×16	I300×200×10×16	I300×200×10×16	I170×170×10×12
	10-12	I350×230×10×16	I400×260×14×18	I300×240×12×18	I300×240×12×18	I170×170×12×14
	7-9	I350×280×10×16	I450×300×14×20	I300×240×12×18	I300×240×12×18	I180×180×12×14
	4-6	I450×300×12×18	I500×340×14×22	I350×240×12×18	I350×240×12×18	I190×190×12×14
	1-3	I450×300×12×20	I500×400×16×25	I350×240×12×18	I350×240×12×18	I190×190×12×14
EK-8-18 EV-8-18	16-18	I300×230×10×16	I300×230×10×16	I350×200×12×16	I350×200×12×16	I170×170×10×12
	13-15	I350×230×10×16	I450×250×14×16	I350×200×12×16	I350×200×12×16	I170×170×12×14
	10-12	I350×280×12×18	I450×330×14×20	I350×240×12×18	I350×240×12×18	I180×180×12×14
	7-9	I450×330×12×18	I500×340×14×22	I350×240×12×18	I350×240×12×18	I190×190×12×14
	4-6	I450×330×12×20	I550×400×16×25	I350×250×12×18	I350×250×12×18	I190×190×14×14
	1-3	I450×350×14×22	I700×450×16×28	I350×250×12×18	I350×250×12×18	I190×190×14×14

Appendix 2 Member sections of archetypes with seismic precautionary intensity 9

Name	Story	Exterior column	Interior column	Exterior beam	Interior beam	Brace
EK-9-6 EV-9-6	4-6	I300×250×12×16	I350×250×12×16	I400×220×10×14	I400×220×10×14	I170×170×8×12
	1-3	I350×250×12×16	I450×280×12×18	I400×220×10×14	I400×220×10×14	I190×190×12×12
EK-9-9 EV-9-9	7-9	I300×250×12×16	I350×250×12×16	I300×210×12×18	I300×210×12×18	I170×170×8×12
	4-6	I350×250×12×16	I450×250×12×18	I300×220×12×18	I300×220×12×18	I180×180×12×12
	1-3	I350×280×12×16	□500×500×22×22	I300×220×12×18	I300×220×12×18	I190×190×12×12
EK-9-12 EV-9-12	10-12	I300×250×12×16	I350×250×12×16	I300×200×10×16	I300×200×10×16	I170×170×8×12
	7-9	I350×250×12×16	I450×250×12×18	I300×200×10×16	I300×200×10×16	I170×170×10×12
	4-6	I350×280×12×16	□500×500×20×20	I300×240×10×18	I300×240×10×18	I180×180×12×12
	1-3	I350×300×12×18	□500×500×22×22	I300×240×10×18	I300×240×10×18	I190×190×12×12
EK-9-15 EV-9-15	13-15	I300×250×12×16	□400×400×18×18	I300×200×12×18	I300×200×12×18	I170×170×10×12
	10-12	I350×250×12×18	□400×400×18×18	I300×240×12×18	I300×240×12×18	I170×170×12×14
	7-9	I350×280×12×18	□450×450×18×18	I300×240×12×18	I300×240×12×18	I180×180×12×14
	4-6	I450×300×12×18	□550×550×20×20	I350×240×12×18	I350×240×12×18	I190×190×12×14
	1-3	□500×500×20×20	□600×600×22×22	I350×240×12×18	I350×240×12×18	I200×200×14×14
EK-9-18 EV-9-18	16-18	I300×250×10×16	□350×350×18×18	I350×200×12×18	I350×200×12×18	I170×170×14×14
	13-15	I350×250×10×16	□350×350×18×18	I350×200×12×18	I350×200×12×18	I180×180×16×16
	10-12	I350×280×12×18	□400×400×20×20	I350×240×12×18	I350×240×12×18	I200×200×16×16
	7-9	I450×330×12×18	□450×450×20×20	I350×240×12×18	I350×240×12×18	I220×220×16×16
	4-6	I450×330×12×20	□550×550×25×25	I350×250×12×18	I350×250×12×18	I230×230×16×16
	1-3	□550×550×20×20	□650×650×25×25	I350×250×12×18	I350×250×12×18	I250×250×16×16
EK-9-24 EV-9-24	22-24	□350×350×18×18	□350×350×18×18	I480×300×18×22	I480×300×18×22	I200×200×20×20
	19-21	□450×450×20×20	□450×450×20×20	I480×300×18×22	I480×300×18×22	I210×210×20×20
	16-18	□450×550×20×22	□450×550×20×22	I500×300×18×22	I500×300×18×22	I220×220×20×20
	13-15	□450×550×20×22	□450×550×20×22	I500×300×18×22	I500×300×18×22	I230×230×20×20
	10-12	□450×550×20×22	□450×550×20×22	I550×300×18×22	I550×300×18×22	I240×240×20×20
	7-9	□500×650×25×25	□500×650×25×25	I550×300×18×22	I550×300×18×22	I250×250×20×20
	4-6	□500×700×25×25	□500×700×25×25	I550×300×18×25	I550×300×18×25	I250×250×20×20
	1-3	□550×700×25×25	□550×700×25×25	I550×300×18×25	I550×300×18×25	I260×260×22×22
EK-9-30 EV-9-30	28-30	□400×400×22×22	□400×400×22×22	I550×300×18×22	I550×300×18×22	I260×260×22×22
	25-27	□450×500×22×22	□450×500×22×22	I550×300×18×22	I550×300×18×22	I260×260×22×22
	22-24	□600×700×25×25	□600×700×25×25	I550×300×18×25	I550×300×18×25	I300×300×25×25
	19-21	□600×700×25×25	□600×700×25×25	I550×300×18×25	I550×300×18×25	I300×300×25×25
	16-18	□600×700×25×25	□600×700×25×25	I550×300×18×25	I550×300×18×25	I320×320×25×25
	13-15	□600×700×25×25	□600×700×25×25	I550×300×18×25	I550×300×18×25	I320×320×25×25
	10-12	□600×750×25×25	□600×750×25×25	I550×300×20×25	I550×300×20×25	I340×340×25×25
	7-9	□600×800×25×25	□600×800×25×25	I550×300×20×25	I550×300×20×25	I340×340×25×25
	4-6	□600×800×25×25	□600×800×25×25	I600×300×20×25	I600×300×20×25	I360×360×25×25
	1-3	□600×800×25×25	□600×800×25×25	I600×300×20×25	I600×300×20×25	I360×360×25×25

Appendix 3 Collapse analysis results of EBSFs with seismic precautionary intensity 8

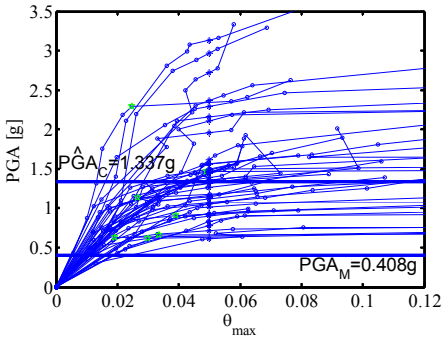

(a) IDA curves

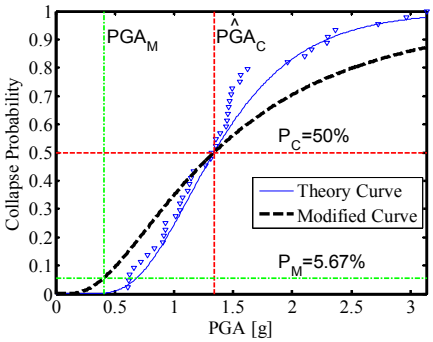

(b) Collapse fragility curve

Fig. A1 Collapse analysis results of EK-8-9

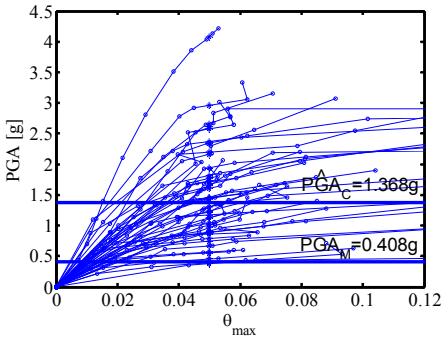

(a) IDA curves

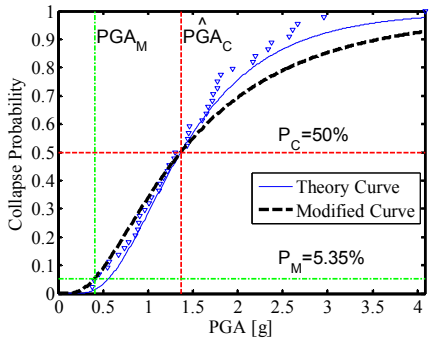

(b) Collapse fragility curve

Fig. A2 Collapse analysis results of EK-8-12

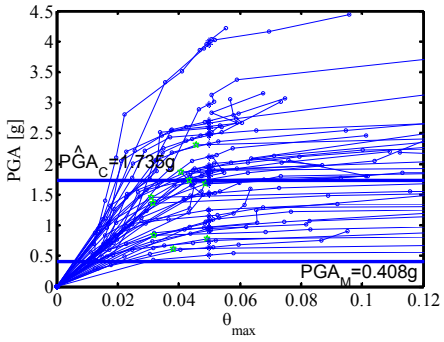

(a) IDA curves

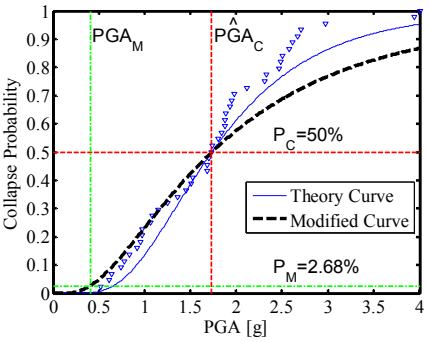

(b) Collapse fragility curve

Fig. A3 Collapse analysis results of EK-8-15

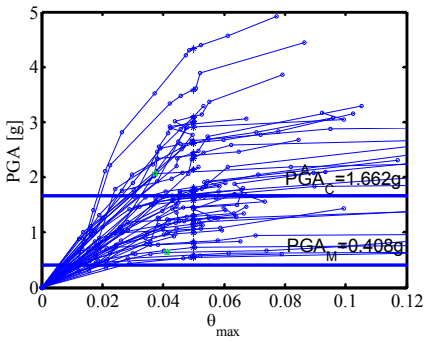

(a) IDA curves

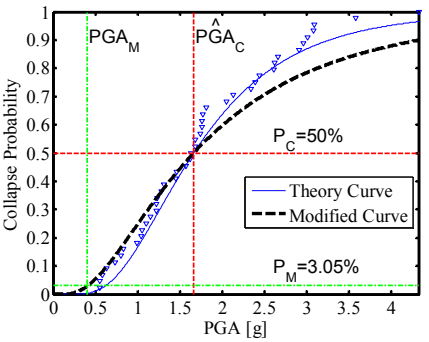

(b) Collapse fragility curve

Fig. A4 Collapse analysis results of EK-8-18

Appendix 3 Continued

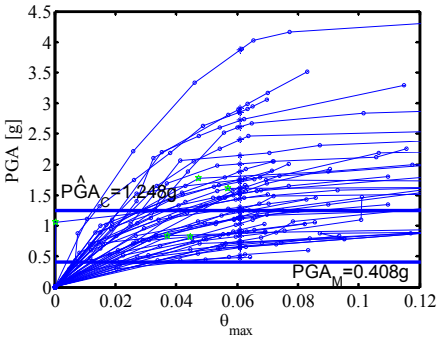

(a) IDA curves

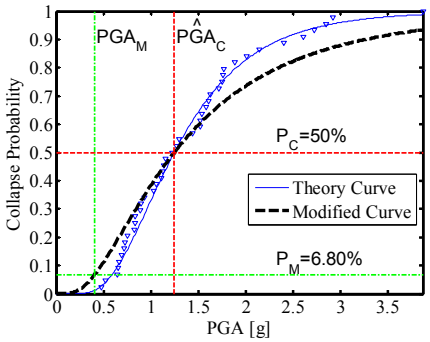

(b) Collapse fragility curve

Fig. A5 Collapse analysis results of EV-8-6

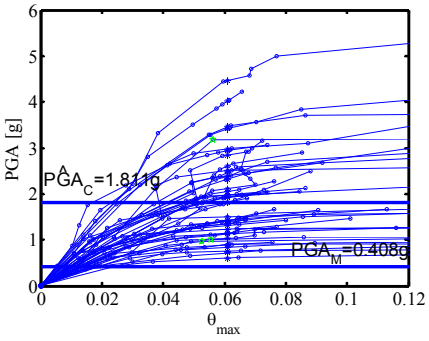

(a) IDA curves

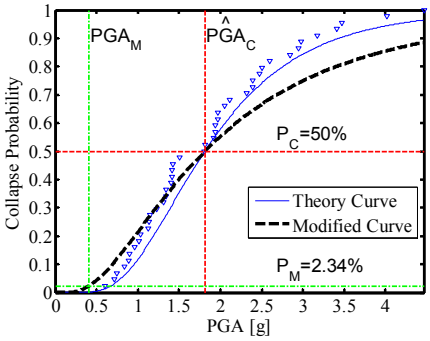

(b) Collapse fragility curve

Fig. A6 Collapse analysis results of EV-8-9

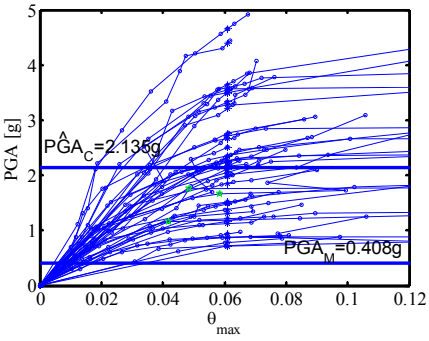

(a) IDA curves

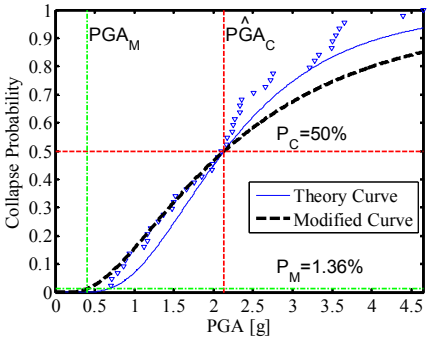

(b) Collapse fragility curve

Fig. A7 Collapse analysis results of EV-8-12

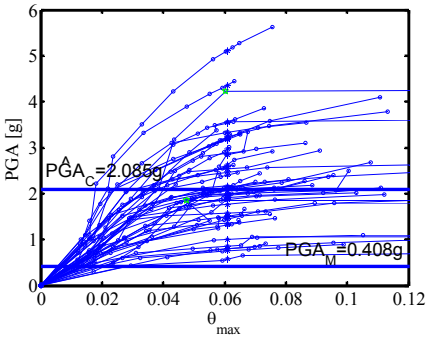

(a) IDA curves

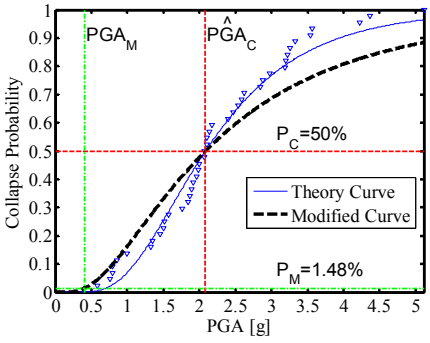

(b) Collapse fragility curve

Fig. A8 Collapse analysis results of EV-8-15

Appendix 3 Continued

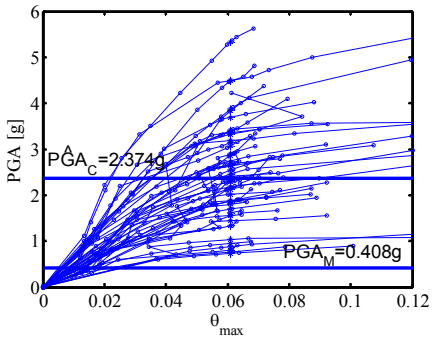

(a) IDA curves

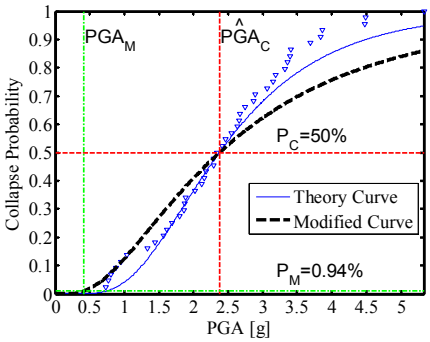

(b) Collapse fragility curve

Fig. A9 Collapse analysis results of EV-8-18

Appendix 4 Collapse analysis results of EBSFs with seismic precautionary intensity 9

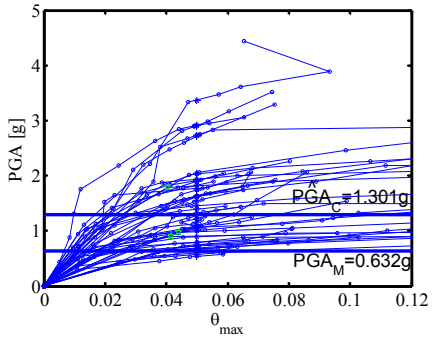

(a) IDA curves

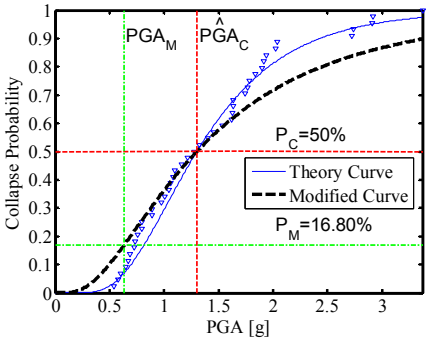

(b) Collapse fragility curve

Fig. A10 Collapse analysis results of EK-9-6

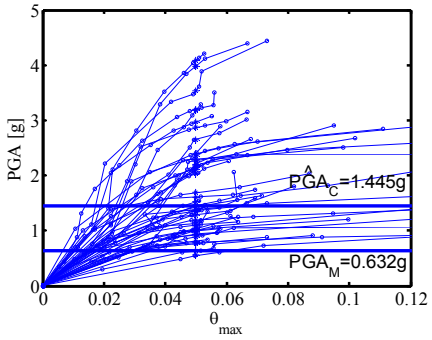

(a) IDA curves

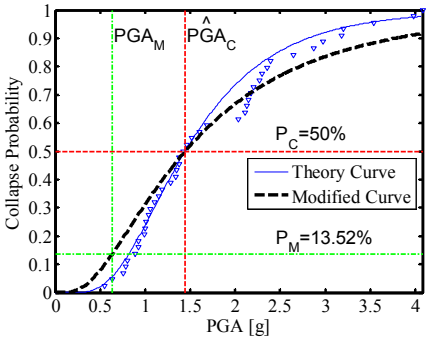

(b) Collapse fragility curve

Fig. A11 Collapse analysis results of EK-9-9

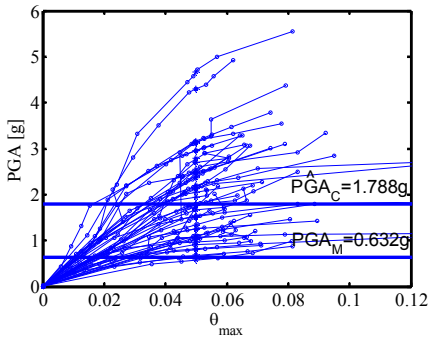

(a) IDA curves

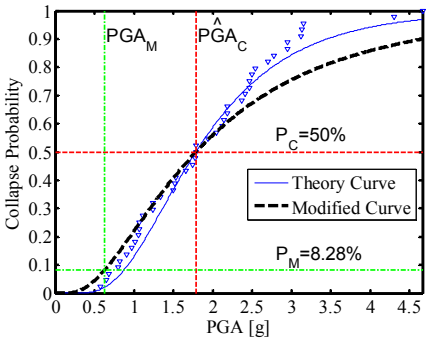

(b) Collapse fragility curve

Fig. A12 Collapse analysis results of EK-9-12

Appendix 4 Continued

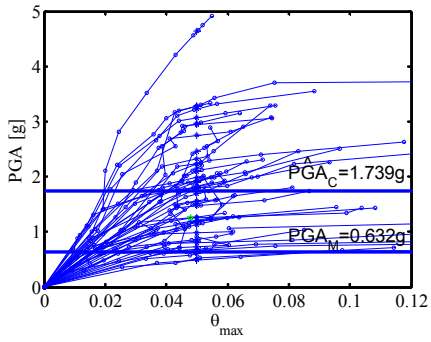

(a) IDA curves

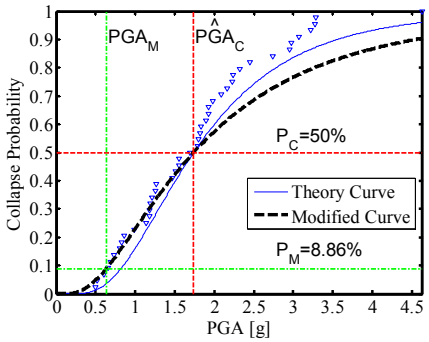

(b) Collapse fragility curve

Fig. A13 Collapse analysis results of EK-9-15

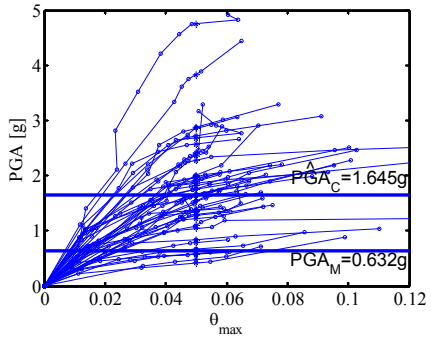

(a) IDA curves

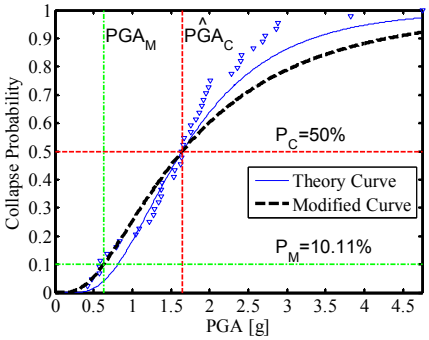

(b) Collapse fragility curve

Fig. A14 Collapse analysis results of EK-9-18

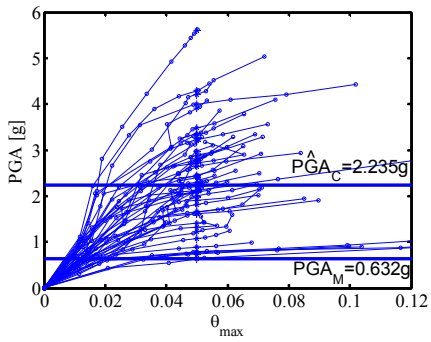

(a) IDA curves

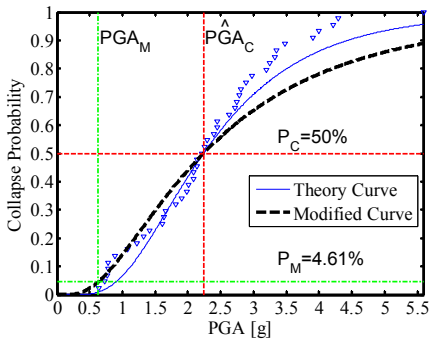

(b) Collapse fragility curve

Fig. A15 Collapse analysis results of EK-9-24

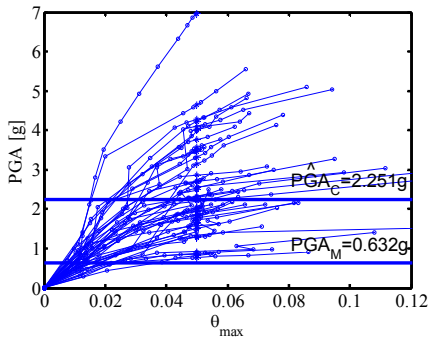

(a) IDA curves

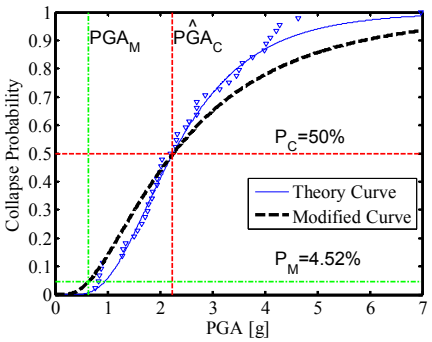

(b) Collapse fragility curve

Fig. A16 Collapse analysis results of EK-9-30

Appendix 4 Continued

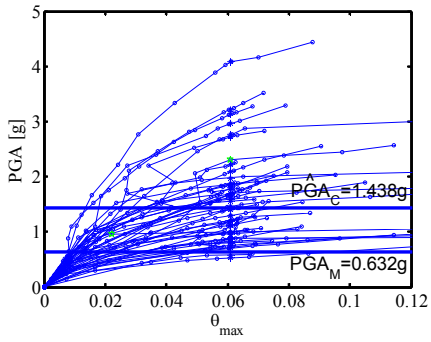

(a) IDA curves

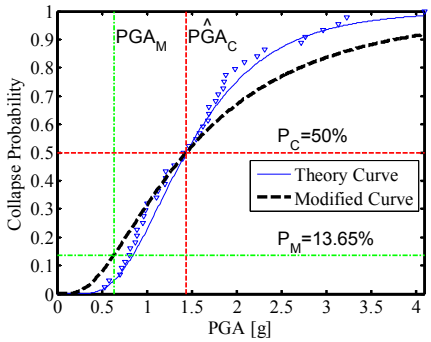

(b) Collapse fragility curve

Fig. A17 Collapse analysis results of EV-9-6

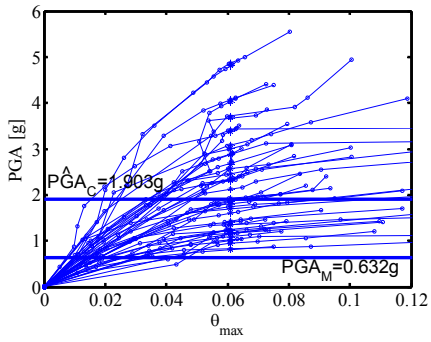

(a) IDA curves

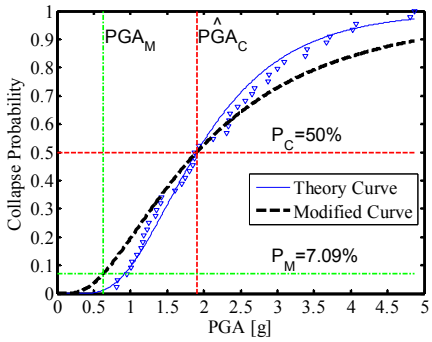

(b) Collapse fragility curve

Fig. A18 Collapse analysis results of EV-9-9

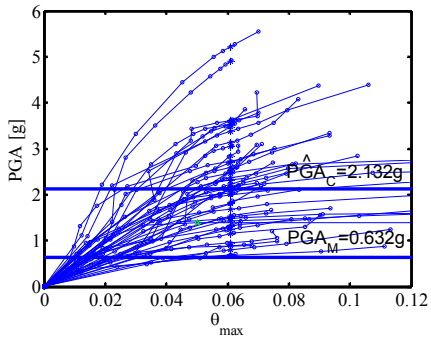

(a) IDA curves

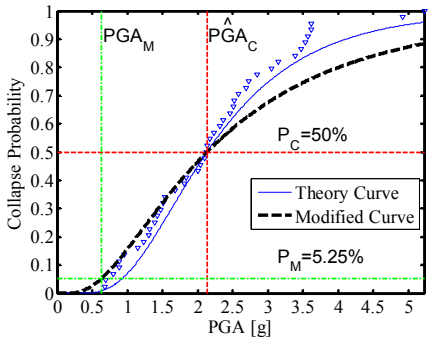

(b) Collapse fragility curve

Fig. A19 Collapse analysis results of EV-9-12

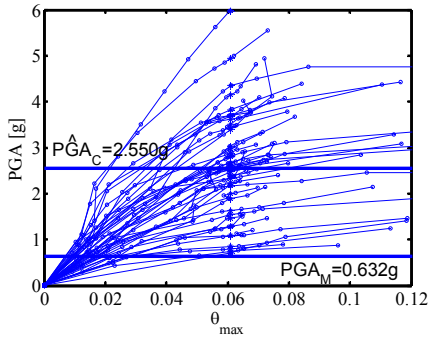

(a) IDA curves

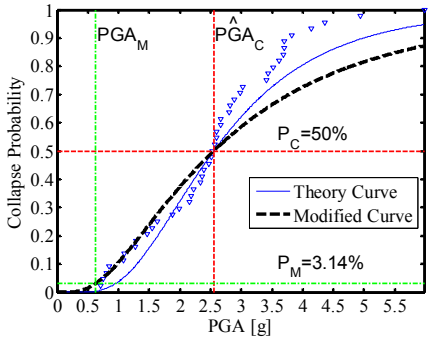

(b) Collapse fragility curve

Fig. A20 Collapse analysis results of EV-9-15

Appendix 4 Continued

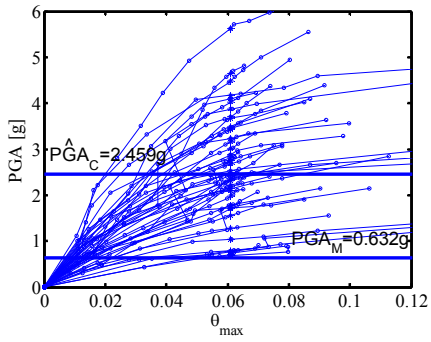

(a) IDA curves

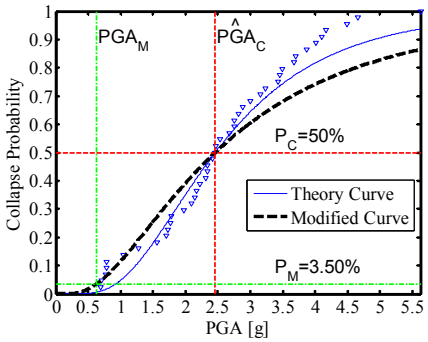

(b) Collapse fragility curve

Fig. A21 Collapse analysis results of EV-9-18

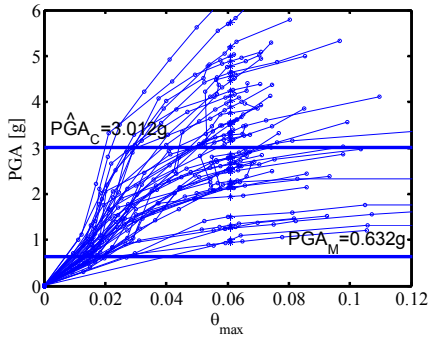

(a) IDA curves

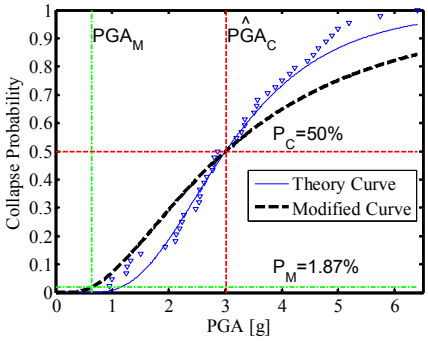

(b) Collapse fragility curve

Fig. A22 Collapse analysis results of EV-9-24

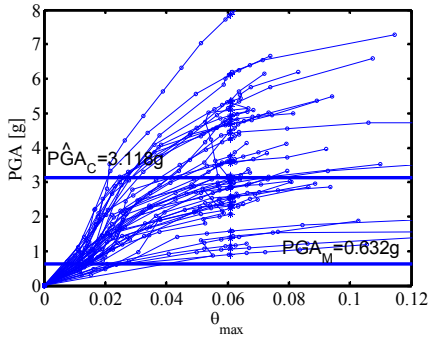

(a) IDA curves

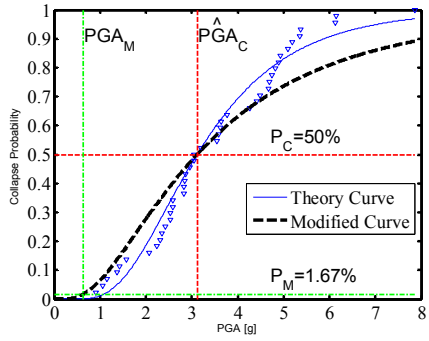

(b) Collapse fragility curve

Fig. A23 Collapse analysis results of EV-9-30